Candidate Planets in the Habitable Zones of *Kepler* Stars

Eric Gaidos

Department of Geology and Geophysics, University of Hawai'i at Mānoa, Honolulu, HI 96822

gaidos@hawaii.edu

Received ______________; accepted ______________

Submitted to *The Astrophysical Journal* on 10 January 2013

arXiv:1301.2384v1 [astro-ph.EP] 11 Jan 2013

ABSTRACT

A Bayesian analysis was used to determine the host star parameters of 2740 candidate and confirmed *Kepler* transiting planets and estimate the probability p_{HZ} that a planet lies within its star's habitable zone, i.e., that the incident stellar irradiation lies between the threshholds for the runaway wet greenhouse and polar CO_2-condensing "snowball" climate states. This analysis is based on photometry from the *Kepler* Input Catalog, an ensemble of Dartmouth Stellar Evolution Program models, and priors for stellar mass, age, metallicity, distance, as well as a constraint from the duration of the planet transit, and yields probability density functions for stellar parameters with which confidence intervals of planet radius and incident stellar flux as well as p_{HZ} are calculated. Fifty-two planets have $p_{HZ} > 0.5$ and a most probable stellar irradiation within the habitable zone limits. Five of these have estimated radii less than twice the Earth, but the majority are super-Earth to Neptune size, and 8 are gas giants which could host habitable exomoons. Another is possibly not a planet, but a brown dwarf or ultracool star. The planet candidate most resembling Earth in terms of size and irradiation is KOI 3010.01, which orbits a late K or early M dwarf. Parallaxes from the *Gaia* mission will reduce errors in planet radius and irradiance by at least a factor of 5, permitting definitive assignments of transiting planets to habitable zones of *Kepler* stars and, eventually, studies of any correlations of planet properties with position in those zones.

Subject headings: planetary systems — techniques: transit surveys — astrobiology

1. Introduction

The *Kepler* mission was launched in March 2009 with a mission to find Earth-size planets in the circumstellar "habitable zone" (HZ) of solar-type stars (Borucki et al. 2010). Broadly speaking, the HZ is considered the range of orbital semimajor axes over which the surface temperature on an Earth-like planet would permit liquid water. A more narrow definition is that it is the range of stellar incident flux between the runaway "wet" greenhouse limit - beyond which a water-vapor saturated N_2-CO_2 atmosphere cannot radiate, and the CO_2 condensation limit below which atmospheric CO_2 - the primary greenhouse gas after H_2O in an Earth-like atmsophere - condenses at the poles (Kasting et al. 1993; Ishiwatari et al. 2007). This definition is subject to assumptions about planetary albedo, orbital eccentricity and obliquity Williams & Pollard (2003), extent of oceans (Abe et al. 2011), and composition of the atmosphere (Pierrehumbert et al. 2011).

Borucki et al. (2011), assuming an Earth-like Bond albedo of 0.3, published a catalog of 54 (out of 1235) candidate planets or *Kepler* Objects of Interest (KOIs) with equilibrium emitting temperatures between 273 and 373 K. Kaltenegger & Sasselov (2011), noting the importance of albedo, specifically cloud cover, to equilibrium temperature, computed inner and outer HZ boundaries based on the stellar irradiation criteria derived by Selsis et al. (2007) for high H_2O and high CO_2 atmospheres, respectively. They identified 76 possible habitable planets, depending on the assumed fractional cloud cover. They found that many of the Borucki et al. (2011) candidates were too hot for this habitability criterion and pointed out that errors in stellar parameters contribute most to the uncertainty of whether a planet orbits within the HZ.

Subsequently, a larger sample of 2300 KOIs, including some that have been confirmed, was released (Batalha et al. 2012). Stellar parameters for KOI hosts, i.e., mass M_* and radius R_*, were determined by fitting Yale-Yonsei model isochrones (Demarque et al. 2004) to values of effective temperature (T_*), surface gravity ($\log g$), and metallicity ([Fe/H]). The latter were derived from the photometry of the *Kepler* Input Catalog (KIC) and a model of stellar populations and Galactic structure (Brown et al. 2011). The Batalha et al. (2012) estimates of mass and radii assumed gaussian-distributed errors and employed standard deviations derived from a comparison between KIC-derived parameters and spectroscopic values. They revised the Brown et al. (2011) estimates of $\log g$ and R_* for many stars. Batalha et al. (2012), assuming an albedo of 0.3 and full redistribution of heat over a planet's surface, identified 46 candidates with 185K $< T_{eq} <$ 303K.

However, the Brown et al. (2011) stellar parameters themselves are uncertain and, in some aspects, problematic. The vast majority of *Kepler* stars do not have measured parallaxes, at least for now. KIC-derived effective temperatures are about 200 K hotter than estimates based on the infrared flux method and KIC photometry must be corrected to place it in the Sloan system (Pinsonneault et al. 2012). Moreover, errors in stellar parameters can be strongly non-gaussian, particularly for solar-type stars for which photometry is unable to distinguish between main sequence and evolved (subgiant) stars (Brown et al. 2011; Gaidos & Mann 2013). In such cases, standard deviations have limited utility.

A revised and expanded catalog of 2740 confirmed and candidate planets around 2036 *Kepler* stars was released on 7 January 2012. Here, I identify 52 candidate HZ planets by comparing corrected KIC *grizJHK* photometry with isochrones from the Dartmouth Stellar Evolution database (Dotter et al. 2008). Like Brown et al. (2011), I use Bayesian statistics, but with new priors that describe distributions with mass (IMF), metallicity, age, and distance using recent models of the Galaxy (Vanhollebeke et al. 2009). In addition, the duration and probability of the planet transit itself are used to constrain the radius of the host star (Plavchan et al. 2012). This statistical approach is used to calculate a *probability* that any given planet is in the HZ. A similar approach has been used on *Hipparcos* stars

(Bailer-Jones 2011). Alternative approaches to the use of broad-band photometry to derive stellar parameters are described in Ammons et al. (2006) and Belikov & Röser (2008).

2. Methods

2.1. Algorithm

I compare photometry for each star with sets of synthetic SDSS *grizJHK*$_s$ photometry from the isochrones of the Dartmouth Stellar Evolution Database (DSED) (Dotter et al. 2008). Specifically I compare up to six colors constructed with respect to the r magnitude. According to Bayes theorem, the probability P_i that the ith model (hypothesis) is supported by the photometry is equal to the probability that the colors c_j can be produced by the model, multipled by a prior function p_i. Assuming gaussian-distributed errors in photometry that probability is,

$$P_i = p_i \exp\left[-\sum_j \frac{\left(c_j - k_j E^i_{B-V} - \hat{c}_j\right)^2}{2\sigma_j^2}\right], \quad (1)$$

where the summation is over up to six colors, $\hat{c}_j$ are the synthetic colors, σ_j are photometric errors, k_j is the interstellar reddening coefficient for the color, and E^i_{B-V} is the amount of reddening that is assigned to a particular model and star (see below). The normalization in Eqn. 1 is unimportant as it independent of the models and I seek the model which has the largest value of P. The prior is the product of individual priors for the mass, age, distance, and metallicity of the model, the intervening extinction, and, since at least one planet has been detected around each of these stars, a constraint on stellar radius placed by the duration and probability of a transit (Plavchan et al. 2012).

Photometry and other data for the host stars of the KOIs were extracted from the KIC catalog available at the MAST database. KIC *griz* magnitudes were corrected to the Sloan system using the corrections determined by Pinsonneault et al. (2012). Standard errors for each bandpass were estimated using the expression $\sigma = \sigma_0 10^{(m-m_0)/2.5}$, where $\sigma_0 = 0.02, 0.02, 0.015, 0.015, 0.02, 0.025, 0.02$, and $m_0 = 15, 15, 15.3, 15.3, 13, 11.75, 10.8$, for *rizjHK*, respectively (Brown et al. 2011; Cutri et al. 2003). For *griz* the magnitude m is the *Kepler* magnitude K_p and for JHK_s it is the respective magnitudes. Errors in color were calculated by assuming that errors in individual bandpasses are uncorrelated and adding the two corresponding such errors in quadrature.

Minimization of P with respect to E_{B-V} leads to a formula for the best-fit reddening for each model:

$$E_{B-V} = \frac{\sum_j k_i \left(c_j - \hat{c}_j\right)/\sigma_j^2}{\sum_j k_j^2/\sigma_j^2} \tag{2}$$

I adopted extinction coefficients A of 3.758 (g), 2.565 (r), 1.874 (i), 1.377 (z), 0.272 (J), 0.173 (H), and (K), based on Girardi et al. (2005) and Chen et al. (2007).

I used the DSED interpolator tool to construct a grid of isochrones with [Fe/H] $\in [-1.5, +0.5]$, spaced by 0.1 dex, $\alpha/Fe \in [-0.2, +0.4]$, spaced by 0.2, and ages $\in [1, 12]$ Gyr. All models used a helium fraction $Y = 0.245 + 1.5Z$, where Z is the total heavy element abundance. I further restricted the selection to stars with initial masses between 0.1 and 2 solar masses, as late M and O, B, and early A-type stars are absent from the *Kepler* target list (Batalha et al. 2010). This restriction reduced the total number of models considered to 657,347.

Once the best-fit model with the maximum P was found, additional models (typically a few dozen) with neighboring (difference less than 1.5 times the grid spacing) values of mass, age, [Fe/H], [α/Fe] were identified. A set of 100 linear interpolations between the best fit model and each of these neighboring models was made and probablities calculated using Eqn. 1. The interpolation yielding the highest value of P was recorded.

2.2. Prior functions

Priors essentially weight each DSED model, i.e. each combination of initial mass, metallicity, and age. No prior is imposed on the allowed range of α/Fe between -0.2 and +0.4. The distance modulus for each star/combination is computed in the r-band, i.e. $\mu_r = r - A_r E_{B-V} - \hat{M}_r$. As a prior for initial stellar masses I adopt the tripartate initial mass function (IMF) of Kroupa (2002). Priors for age, metallicity, and distance modulus $\mu = m - M$ were constructed using the distributions of dwarf stars ($\log g > 4$) with $K_p < 16$ synthesized using TRILEGAL . The simulated population was restricted to dwarfs to reflect the criteria of the selection of *Kepler* targets (Batalha et al. 2010). The (mostly default) values for key TRILEGAL parameters are the same as used in Gaidos & Mann (2013).

The resulting distributions (Fig. 1) have a median metallicity of -0.13, median age of 3.9 Gyr, and median $\mu = 11.2$ ($\sim$1740 pc). The age distribution is complex because the population includes halo stars, which form 11-12 Gyr ago, and disk stars, which start forming 9 Gyr in these simulations. The star formation rate in the disk is modeled as two steps, with the second occurring at about the epoch of the Sun's formation. The paucity of stars younger than 1 Gyr is partly due to the fact that the *Kepler* field probes the stellar population that is $>$ 100 pc above the Galactic plane. Of course, stellar ages, metallicities, and distances are interrelated, but here they are used separately, providing broad constraints on the possible ranges of stellar parameters. The distance distribution is particularly important in allowing the finite scale height of the Galactic disk to prevent Malmquist bias from selecting arbitrarily distant and luminous stars.

The *Kepler* field is $\sim$10 degrees wide and close to the Galactic plane ($b \sim 13$ deg), so the stellar populations that are probed will vary significantly across the field. Using TRILEGAL, I synthesized the stellar population over a square degree centered at each of the 85 *Kepler* CCD fields. Only those synthetic populations for CCD field centers with b

within 0.5 deg of a given *Kepler* star (about 10% of the total) were used to calculate priors for age, metallicity, and distance.

A prior for extinction E_{B-V} necessarily involves information about both the distribution of stellar distances, and the distribuiton of dust along the line of sight. However, by assuming that the spatial distributions of stars and dust along the line of sight is the same, the prior becomes particularly simple: a uniform distribution between 0 and total (∞) extinction along the line of sight (see Appendix A). I adopted the Schlegel et al. (1998) Galactic reddening maps and interpolated the total extinction at the coordinates each star using the IDL tools provided by the Princeton website. Models with optimal E_{B-V} values outside this range are not disallowed, but reddening is limited to $0 - E_{B-V}(\infty)$ and the models are penalized for the resulting disagreement between measured and model colors (Eqn. 1).

2.3. Constraints from the planet transit

The transit duration τ and orbital period P_K of a transiting planet constrain stellar density (Plavchan et al. 2012) and can be used as an additional prior for stellar models. In the case of *Kepler* low-cadence data, the constraint is weakened by a lack of information about the orbit, specifically independent determination of the orbital eccentricity and the transit impact parameter. The transit duration D is:

$$D = \tau^{2/3} P_K^{1/3} \frac{\sqrt{(1-e^2)(1-b^2)}}{1 + e\cos\phi}, \tag{3}$$

where the stellar free-fall time is $\tau = 2\sqrt{\hat{R}_*^{\,3}/(\pi G \hat{M}_*)}$, G is the gravitational constant, e is the orbital eccentricity, ϕ is the argument of periastron relative to the line of sight to the star, and b is the impact parameter. Given D and P_K and a value for τ for each stellar model, e can be written as a function of b and ϕ:

$$e(b, \phi, \Delta) = \frac{\sqrt{(1 - b^2)\left(1 - b^2 - \Delta^2 \sin^2 \phi\right)} - \Delta^2 \cos \phi}{1 - b^2 + \Delta^2 \cos^2 \phi}, \tag{4}$$

where $\Delta \equiv D/(\tau^{2/3} P^{1/3})$. The eccentricity was calculated over a uniform grid of $b \in [0, 1]$ and $\phi \in [0, 2\pi]$. Each value of e was assigned a probability, i.e. values not $\in [0, 1]$ are assigned zero and others are assigned probabilities from a prior distribution of e. A Rayleigh distribution,

$$\rho(e) = \frac{e}{\sigma^2} e^{-e^2/(2\sigma^2)}, \tag{5}$$

is assumed. Such a distribution has been used in a previous analysis of *Kepler* transit durations (Moorhead et al. 2011) and is motivated by dynamical theory (Jurić & Tremaine 2008). Then the prior for the ith model from the duration of the transit is

$$p_i = \frac{1}{2\pi} \int_0^1 db \int_0^{2\pi} d\phi \, \rho\left(e(b, \phi; \Delta_i)\right). \tag{6}$$

To account for finite errors in transit duration, the prior can be calculated using multiple Monte Carlo-generated values of D is repeated and then averaged. In the case of a multi-planet system $j = 1...N$, the product of the individual transit duration priors $\Pi_j p_{ij}(\Delta_{ij})$ was used. A value of $\sigma = 0.2/\sqrt{\pi/2}$ for the dispersion in eccentricities was used based on (Moorhead et al. 2011). Figure 2 plots ρ for 4 values of σ. The choice of prior for e, although motivated by *Kepler* observations, is not unique and indeed a more refined distribution would include dependencies on planet mass, orbital period, and the age of the system (Wang & Zhou 2011).

2.4. Probability that a planet orbits in the habitable zone

Orbit-averaged irradiation is only weakly dependent on eccentricity for near-circular orbits. I assume near-circular orbits in which case the mean irradiation in terrestrial units is

$$\bar{I} \approx \frac{\hat{L}_*}{L_\odot} \left(\frac{P_K}{365.24\ \mathrm{d}} \right)^{4/3} \left(\frac{\hat{M}_*}{M_\odot} \right)^{2/3} . \tag{7}$$

A planet is defined to be in the HZ if $I_{out} < \bar{I} < I_{in}$, where the irradiance of the inner edge of the HZ for a 50% cloud-covered planet with efficient heat re-distribution is (Selsis et al. 2007)

$$I_{in} = \left[0.68 - 2.7619 \times 10^{-5} \Theta - 3.8095 \times 10^{-9} \Theta^2 \right]^{-2} , \tag{8}$$

and the outer edge is:

$$I_{out} = \left[1.95 - 1.3786 \times 10^{-4} \Theta - 1.4286 \times 10^{-9} \Theta^2 \right]^{-2} , \tag{9}$$

where $\Theta \equiv \hat{T}_* - 5700$.

I determine whether a planet is in the HZ for each set of model stellar parameters $\hat{M}_*$,$\hat{L}_*$, and $\hat{T}_*$ with associated probability P_i. The probability p_{HZ} that the planet is in the HZ is then:

$$p_{HZ} = \frac{\sum\limits_{i \in HZ} P_i}{\sum\limits_{i} P_i} \tag{10}$$

I consider candidate habitable planets (or planets that may have habitable satellites) as having $p_{HZ} > 0.5$ and having a most probable value of $\bar{I}$ (with highest P) satisfying $I_{out} < \bar{I} < I_{in}$.

3. Results

3.1. Comparison with spectroscopic parameters

Accurate estimates of stellar effective temperature T_* and radius R_* are crucial to assessing whether a planet is in the HZ, as together these largely determine the luminosity of the host star and the irradiance experienced by the planet on a given orbit. The inferred radius of a transiting planet also scales linearly with the estimated radius of the host star. The radii of distant *Kepler* stars cannot be directly measured, but spectroscopic values of T_* and surface gravity $\log g$, the latter related to R_*, are available for some *Kepler* stars with planets (Bruntt et al. 2012; Buchhave et al. 2012, ; Mann et al., in prep.). Figs. 3 and 4 compare photometry-based values of T_* and $\log g$ with reported spectroscopic values. Photometric values for solar-type stars where all 6 colors are available average 210 K higher than spectroscopic values (Fig. 3). Pinsonneault et al. (2012) found that both the original KIC temperatures *and* spectroscopic estimates were ∼215 K cooler than determinations using the infrared flux method (IRFM). Thus the new photometric estimates are in line with IRFM values. The offset between photometric and spectroscopic temperatures is less (∼100 K) for M dwarfs; spectroscopic temperatures for these stars (Mann et al., in prep.) were determined by comparing spectra to synthetic spectra from PHOENIX/BT-SETTL models (Allard et al. 2011) and tuning the comparison using the temperature estimates of Boyajian et al. (2012).

After removing the 210 K offset, the standard deviation between photometric and spectroscopic values of T_* for solar-type stars is $\sigma = 205$ K. This equals the performance of the analysis of Bailer-Jones (2011), but without the benefit of parallax. Photometric T_* for several stars is significantly ($> 2\sigma$) lower than spectroscopic estimates. All but one of these are missing either i- or z-band photometry, or both. The importance of these bandpasses is not surprising as they are the only source of information in the wavelength range 0.7μm $< \lambda < 1.1\mu$m, just beyond the peak in emission from most of these stars, a spectral feature which most strongly constrains T_*.

There are also 7 stars which have significantly ($> 2\sigma$) hotter photometric estimates of T_*; only one of these has missing photometry. One of these has a spectroscopic temperature estimated using the method applied to M dwarfs (Mann et al., in prep.) but does not have the spectrum of an M dwarf, and thus its spectroscopic temperature is unreliable. The reason(s) for the discrepancy among the remaining six are unclear. One possibility is that the photometric source is a blend resolved by spectroscopy, or that the transit signal itself may be coming from a component of a blend which is dissimilar to the source of most of the light, and consequently the transit duration prior is skewing the stellar parameters.

Photometry-based estimates of $\log g$ are more discrepant with spectroscopic values, although an overall correlation is apparent (Fig. 4). About half of the most discrepant cases lack photometry in at least one bandpass, although many stars with missing photometry are assigned surface gravities close to the spectroscopic estimates. Although photometric colors involving the SDSS u (Lenz et al. 1998) and z (Vickers et al. 2012) bands can be used to discriminate between hotter main sequence and evolved stars, photometry is a much blunter tool to separate solar-type stars by luminosity class. While my analysis may only marginally improve this situation, it does quantify the uncertainties.

Among the KOI host star with reported spectroscpic parameters are those with candidate HZ planets discussed below (§3.2). Buchhave et al. (2012) report spectroscopic parameters for 3 of the stars in Table 1, including *Kepler*-22b. The photometric values of T_* are up to 200 K warmer than the corresponding spectroscopic estimates (Fig. 3). Muirhead et al. (2012) obtained infrared (K-band) spectra for 6 of these HZ candidates and Mann et al. (in prep.) obtained visible-wavelength spectra for 10, including 4 of the Muirhead et al. (2012) targets (Table 1). The spectra show that all 12 are late K- or early

M-type dwarfs. Two (KOIs 812.03 and 854.01) were previously identified by Muirhead et al. (2012) as orbiting in the star's habitable zone. In general, the photometric temperatures are ∼100 K warmer than the spectroscopic values of Mann et al, which are in turn warmer than those of Muirhead et al. (2012) (see also Fig. 3). The most discrepant case is KOI 2418.01, for which the photometric estimate of T_* is 459 K hotter than that of Mann et al., who find $T_* \approx 3500$K. The spectral type is M0.5, which is marginally consistent with either of these values of T_*. One explanation for the discrepancy is confusion with another star - there is a source about 4 arc-sec away in high-resolution UKIRT J-band imaging. The case of M dwarf stars is discussed in §4.

3.2. Habitable Planets

Of the 2740 confirmed and candidate KOIs, the analysis of 1 star (KIC 7746948 hosting KOIs 326.01 and 326.02) failed, as it is missing an r magnitude and therefore cannot be analyzed by this procedure. Figure 5 is a Hertzsprung-Russell diagram of the other 2035 KOI host stars. The stars hosting HZ candidates are indicated in black and only their associated errors in luminosity are plotted (for clarity). Seven HZ candidates (KOIs 375.01, 422.01, 435.02, 490.02, 1096.01, 1206.01, and 1421.01) were excluded because their reported orbital periods have large uncertainties, being based on the duration of a single transit and the assumption of a circular orbit). The remaining HZ candidates have host stars with effective temperatures from 3500 K (early M-type) to 6100 K (late F-type). With the exception of KIC 6766634 (hosting KOI 1375.01), which is missing an $r - z$ color, all HZ candidate host stars have all 6 photometric colors. Luminosities for some host stars have very high upper bounds because neither the photometric colors nor the priors can rule out the possibility that they are evolved with 95% confidence. But all are most likely to be dwarfs except for two of the hottest host stars (for KOIs 1168.01 and 1574.02), which have probabilities of 77 and 53% of being evolved stars, i.e. $\log g < 4.2$. All are designated as slighly metal poor, most likely the result of the metallicity prior (§2.2).

The 52 candidates with $p_{HZ} > 0.5$ and most probable incident stellar irradiation in the HZ limits are listed in Table 1 and plotted in Figs. 6 and 7. Thirty-four were previously identified as possible HZ planets by Borucki et al. (2011), Kaltenegger & Sasselov (2011), and/or Batalha et al. (2012). Most, but not all, of the others are candidates from the 1-7-2012 release. The candidate around the brightest host star, KOI 87.01/*Kepler*-22b was previously flagged by Borucki et al. (2011) and Kaltenegger & Sasselov (2011) and confirmed by Borucki et al. (2012). The photometric estimate of effective temperature (5735 K) is consistent with two spectroscopic estimates (5518 and 5642 K), the inferred luminosity is slightly higher $0.9L_{\odot}$ compared to $0.79L_{\odot}$, and the inferred age of 8 Gyr is consistent with slow rotation and low flux in the core of the Ca II H and K lines (Borucki et al. 2012). The inferred stellar mass is identical ($0.93M_{\odot}$) that determined by astroseismology. The preferred planet radius is $2.32\mathrm{R}_{\oplus}$and is within the errors of the previously published value of $2.38 \pm 0.13\mathrm{R}_{\oplus}$, although the 95% confidence interval for this star is large.

KOI 250.04 is not (yet) a confirmed planet but is the outermost known member of the 4-planet *Kepler*-26 system containing two components (b and c) confirmed by TTV analysis (Steffen et al. 2012) and a fourth candidate (KOI 250.03) on the innermost orbit. The orbital period of KOI 250.04 (P_K = 46.83 d) is suspicously close to one half of the period of a TTV signal seen near 90 d (Steffen et al. 2012). This analysis indicates that the host star of these planets has $T_* = 4072$ K, i.e. is a late K dwarf. This is confirmed by two moderate-resolution visible-wavelength spectra which return 3996 K and 4067 K and a spectral type of K7.5 (Mann et al. in prep.), and an infrared spectrum which gives $T_* = 3887$K (Muirhead et al. 2012). Steffen et al. (2012) report $T_* = 4500$ K based on an SME analysis (Valenti & Piskunov 1996) of a Keck-HIRES spectrum. However, SME effective temperatures are unreliable for very cool stars such as this. KOI 250.04 has a radius of about $2.4\mathrm{R}_\oplus$, and it is of particular interest because further TTV analysis might constrain its mass.

The distribution with planet radius among these 52 objects peaks in the super-Earth range ($\sim 2.5\mathrm{R}_\oplus$) and decreases with increasing radius, although there appears to be a second group of candidate planets with radii approximately that of Jupiter. Most of the smaller planets orbit lower-mass stars (Fig. 7), a correlation at least partly due to detection bias. Presumably gas giants, these objects are potential hosts for habitable satellites (Kipping et al. 2009; Kaltenegger 2010). The upper limits (95% confidece) on the radii of 6 candidates significantly exceeds the theoretical upper limit for cool Jupiters (Fortney et al. 2010, $R_p \approx 13.5\mathrm{R}_\oplus$,). Using the same approach as the calculation of p_{HZ}, I calculated the probability that a candidate planet's radius is larger than $1.2\mathrm{R}_J$, based on the transit depth and model stellar radii. For each of these 6 objects, there is a $\geq 10\%$ chance that the actual radius does exceed this limit. In 5 of these cases, this can be explained by the very large errors in the radius of the host star (an evolved star cannot be ruled out). The 95% confidence interval in radius of KOI 113.01 extends from $1.3\mathrm{R}_J$ to a clearly non-planetary $0.37R_\odot$. The probability that this object has a radius larger than $1.2R_J$ is 99%, suggesting this is not a planet at all, but an very cool or ultracool dwarf. Batalha et al. (2012) list this KOI as having a "V-shaped" transit lightcurve indicative of an eclipsing binary. Depending on this object's luminosity, it is not inconceivable that any planets orbiting on stable orbits around *it* would be in the HZ of the combined system. All other KOIs in Table 1 have $p(R_P > 1.2R_J) < 0.17$.

KO 3010.01 has a most probable radius of $1.35\pm^{+0.44}_{-0.09}\mathrm{R}_\oplus$, and an irradiance of $\sim$0.81 that received by Earth. Table 1 also includes 6 additional objects of interest with $R_p < 2\mathrm{R}_\oplus$)

planets and $p_{HZ} > 0.1$ (but < 0.5). Five of these orbit late K or early M-type dwarf stars, a figure that supports claims that these stars are the most promising locales to find Earth-size, and Earth-like planets.

3.3. Not-so-habitable planets

Kaltenegger & Sasselov (2011) list 27 planets with semimajor axes between the inner edge (as defined by the onset of a runaway greenhouse) and outer edge of the HZ. Of these, 7 (KOIs 113.01, 465.01, 1008.01, 1026.01, 1134.02, 1168.01, 1232.01, were not retained in the Batalha et al. (2012) catalog. KOIs 1008.01 has a V-shaped transit shapes and 1232.01 has a large radius indicative of an elipsing binary. KOI 1134.02 exhibits "active pixel offset" meaning that the target star is not the source of the transit signal. KOI 1026.01 might be an artifact of systematics in the *Kepler* data (Batalha et al. 2012). KOIs 113.01, 465.01 and 1168.01 were detected only with a single transit in the Borucki et al. (2011) catalog. Of the remaining 20, five (KOIs 139.01, 1099.01, 1423.01, 1439.01, and 1503.01) have $p_{HZ} < 0.5$ and so do not appear in this catalog, although KOI-1423.01 is omitted marginally only so (0.47). KOI 1439.01 is most strongly ruled out ($p_{HZ} = 0.06$) because the revised T_* is 274 K hotter and R_* is 46% larger than the KIC values used by Kaltenegger & Sasselov (2011). The other 15 KOIs are retained in this catalog, along with 5 others from Kaltenegger & Sasselov (2011).

A comparison with the HZ candidates of Batalha et al. (2012) is problematic because they use an equilibrium temperature criterion which is and dependent on the color/effective temperature of the host star. However, of the 24 candidate planets with 185K $< T_{eq} <$300K in Table 8 of Batalha et al. (2012), six (KOIs 119.02, 438.02, 986.02, 1938.01, 2020.01, and 2290.01) have $p_{HZ} < 0.05$ and most probable $< I >$ outside the HZ limits. In each case, this is because the new estimates for T_* are $\geq$200 K hotter than the previously published values, and becuse the most probably estimate of radius is significantly larger.

4. Discussion

Assumptions and biases: My priors do not account for the probability that a planet will transit its host star and be detected by *Kepler*, and thus be included in the KOI catalog. Such selection effects can be important in catalogs of transiting planets and their host stars (Gaidos & Mann 2013). The geometric transit probability R_*/a, where a is the semimajor axis, is proportional to $\tau^{2/3}$ and could be included readily enough: this factor will favor stellar models with larger radii. However, the probability of transit detection is primarily related to transit depth $\delta \approx (R_p/R_*)^2$ and for a given δ, a prior on stellar radius is ultimately a prior on *planet* radius. Some of these KOIs are nearly Earth-size, where the completeness of the *Kepler* survey is still being refined. Other KOIs are at or near theoretical limits of giant planet radii and any prior on stellar radii would have to include scenarios for astrophysical false positives. There are additional, but perhaps minor complexities: the probability of a transit occurring and being detected will also depend on e, ϕ, b, as well as D, the transit duration. For these reasons, I do not include transit detection as a prior.

The derivation of the extinction (Eqn. 2) presumes a linear relationship between extinction in different bandpasses, i.e. that all can be linearly related to reddening E_{B-V}. This is not strictly correct, but is a fair approximation in the limit of small reddening. The median derived E_{B-V} for these stars is only 0.069, corresponding to 0.2 magnitudes of extinction, and the 95 percentile value is 0.18. The distribution of reddening values is shown in Fig. 8. The scale height of dust is smaller than that of stars, and as a result the assumption of identical gas and dust distributions (Appendix A) slightly underestimates the amount of reddening, as well as the temperature and luminosities of *Kepler* stars.

The total number of candidate HZ planets is not sensitive to the precise irradiation limits. Because of detection bias towards short-period orbits, there are essentially no detected planets beyond the HZ (Fig. 6), except perhaps for those detected by only a single transit. For a planet with 100% cloud cover, the runaway greenhouse irradiation limit is 23% higher than the 50% case, but this admits only one additional candidate to the catalog.

The trouble with M dwarfs: The fundamental parameters of M dwarf stars have been a notorious challenge for models because of the difficulty in reproducing the observed mass-radius relation and their complex spectra. The DSED models employed here accurately predicts the radii of the two M dwarfs in the triply eclipsing hierarchical triple system KOI-126 (Feiden et al. 2011). DSED uses the PHOENIX model atmospheres (Hauschildt et al. 1999) for both the stellar surface boundary conditions and to generate synthetic magnitudes. The analysis of Mann et al., in prep., compares the BT-SETTL flavor of PHOENIX models to medium-resolution spectra, hence the consistency between effective temperatures estimates is not entirely surprising. However, not all flavors of PHOENIX are identical, and moreover, Mann et al. calibrated temperatures against the stars analyzed in Boyajian et al. (2012), which have both measured parallaxes and (interferometric) radii. For early M dwarfs, a difference of only ∼100 K in T_* is nevertheless a difference in L_* of about 30%.

Another obstacle is that accurate modeling of the lightcurves of planets transiting M dwarfs must correctly account for significant limb darkening in the *Kepler* pass-band. Erroneous transit durations, acting through the prior described in §2.3, can bias the analysis towards models with erroneous radii: a 10% error in R_* again leads to a ∼30% error in L_*. This is sufficient to move a planet completely outside the HZ, or at least decrease the p_{HZ} of a marginal HZ planet to <50%. A re-analysis of the *Kepler* transit lightcurves with an improved limb-darkening model and re-derivation of the parameters of M dwarf KOI hosts is forthcoming (Mann et al., in prep.)

Stellar parameters based on analysis of photometry are no substitute for values based on high-resolution spectra, as long as the latter are carefully calibrated (e.g., Pinsonneault et al. 2012). However, the median magnitude of the host stars of these planet is $K_p \approx 15.1$, and high-resolution spectroscopy would be very observationally expensive. The object most amenable to followup is, not coincidentally, *Kepler*-22b ($K_p = 11.7$). The next brightest host star is that of KOI 371.01 ($K_p = 12.4$) and the rest are much fainter still and would require significant time on very large telescopes. The analysis presented here does, however, generate a robustly-defined catalog of targets to prioritize such work.

The *Gaia* (originally Global Astrometric Interferometer for Astrophysics) mission, scheduled for launch in October 2013, will obtain parallaxes with a sky-averaged, end-of-mission precision of 25 μas and 40 μas for 15th and 16th magnitude stars, respectively, with somewhat superior performance at the ecliptic latitude ($\sim$66 deg.) of the *Kepler* field (de Bruijne 2012). To assess the potential of *Gaia* to refine the habitable zones of *Kepler* stars and the sizes of the planest that inhabit them, I re-calculated P_i (Eqn. 1) for all models using a prior for distance modulus p_μ based on *Gaia*'s expected precision:

$$p_\mu = \exp\left[-\frac{(\mu - \mu_0)^2}{2\sigma_\mu^2}\right], \tag{11}$$

where μ_0 is the most probable distance modulus from the original analysis, and $\sigma_\mu \approx 8.7 \times 10^{\mu_0/5-4}$ is the uncertainty in distance modulus from a 40 μas precision in parallax. The 95% confidence intervals in radius and stellar irradiance of the 52 HZ candidates were re-calculated and are shown in Fig. 9. The most probable values are not changed, but the fractional errors in radius and irradiance are reduced by a factor of $\sim$5, from a median of 10% and 24%, respectively, to 1.7% and 5%, (equating 95% confidence intervals to 4σ). The largest planets tend to orbit the hottest and most distant stars (Gaidos & Mann 2013) and their parameters have the largest errors. Typically, a few hundred models contribute to the calculation, i.e. retain appreciable P values, but in a few cases the number is a few dozen and finite model grid size may contribute to the error budget. Values of p_{HZ} for 50 of the 52 planets are > 0.97. Spectroscopic values of T_* accurate to 100 K would offer only modest further improvement (1.5% and 4.5% errors, respectively). Because these precisions reach or exceed levels of confidence in the predictions of the stellar models themselves as well as the absolute calibration of the photometry, refinement and verification of these may prove a more cost-efficient avenue for improvement. For example, *Ugri* and H_α photometry of much of the *Kepler* field has been obtained at the Isaac Newton Telescope (Greiss et al. 2012) and *UBV* photometry has been obtained at WIYN (Everett et al. 2012).

With such precision (or better!), it should be possible to locate planets within different realms of the HZ, i.e. near the inner edge, where low CO_2 atmospheres, and possibly high cloud fraction if there is a temperature-cloud feedback, should prevail: or the outer edge, where high CO_2 (von Paris et al. 2013), and possible water cloud-free atmospheres are more likely Candidate HZ planets in multi-planet systems might be confirmed or even have masses determined by TTV. Although such advances may be challenges for planets around faint *Kepler* stars, this analysis offers a preview of the potential for surveys of nearby, more observationally accessible stars, e.g. by the proposed TESS (Deming et al. 2009) and CHEOPS missions.

This research was supported by NSF grants AST-09-08406 and NASA grants NNX10AI90G and NNX11AC33G to EG. The *Kepler* mission is funded by the NASA Science Mission Directorate, and data were obtained from the Mukulski Archive at the Space Telescope Science Institute, funded by NASA grant NNX09AF08G, and the NASA Exoplanet Archive at IPAC. Andrew Mann kindly provided stellar parameters in advance of publication.

REFERENCES

Abe, Y., Abe-Ouchi, A., Sleep, N. H., & Zahnle, K. J. 2011, Astrobiology, 11, 443

Allard, F., Homeier, D., & Freytag, B. 2011, in Astronomical Society of the Pacific Conference Series, Vol. 448, 16th Cambridge Workshop on Cool Stars, Stellar Systems, and the Sun, ed. C. Johns-Krull, M. K. Browning, & A. A. West, 91

Ammons, S. M., Robinson, S. E., Strader, J., Laughlin, G., Fischer, D., & Wolf, A. 2006, ApJ, 638, 1004

Bailer-Jones, C. A. L. 2011, MNRAS, 411, 435

Batalha, N. M., et al. 2010, Astrophys. J., 713, L109

Batalha, N. M., et al. 2012, ArXiv e-prints

Belikov, A. N., & Röser, S. 2008, A&A, 489, 1107

Borucki, W. J., et al. 2010, The Astrophysical Journal, 713, L126

—. 2011, Astrophys. J., 736, article id. 19

—. 2012, The Astrophysical Journal, 745, 120

Boyajian, T. S., et al. 2012, Astrophys. J., 757, 112

Brown, T. M., Latham, D. W. D., Everett, M. E. M., & Esquerdo, G. G. A. 2011, Astron. J., 142, 112

Bruntt, H., et al. 2012, Mon. Not. Royal Astron. Soc., 423, 122

Buchhave, L. a., et al. 2012, Nature, 486, 375

Chen, P.-S., Yang, X.-H., & Zhang, P. 2007, AJ, 134, 214

Cutri, R. M., et al. 2003, 2MASS All Sky Catalog of point sources.

de Bruijne, J. H. J. 2012, Ap&SS, 341, 31

Demarque, P., Woo, J., & Kim, Y. 2004, The Astrophysical Journal Supplement Series, 155, 667

Deming, D., et al. 2009, Publ. Astron. Soc. Pac., 121, 952

Dotter, A., Chaboyer, B., Jevremović, D., Kostov, V., Baron, E., & Ferguson, J. W. 2008, Astrophys. J., 178, 89

Everett, M. E., Howell, S. B., & Kinemuchi, K. 2012, PASP, 124, 316

Feiden, G. a., Chaboyer, B., & Dotter, A. 2011, The Astrophysical Journal, 740, L25

Fortney, J. J., Baraffe, I., & Militzer, B. 2010, in Exoplanets (University of Arizon Press), 397

Gaidos, E., & Mann, A. W. 2013, ApJ, 762, 41

Girardi, L., Groenewegen, M. A. T., Hatziminaoglou, E., & da Costa, L. 2005, A&A, 436, 895

Greiss, S., et al. 2012, AJ, 144, 24

Hauschildt, P., Allard, F., & Baron, E. 1999, The Astrophysical Journal, 512, 377

Ishiwatari, M., Nakajima, K., Takehiro, S., & Hayashi, Y.-Y. 2007, Journal of Geophysical Research, 112, 1

Jurić, M., & Tremaine, S. 2008, ApJ, 686, 603

Kaltenegger, L. 2010, Astrophysical Journal Letters, 712, L125

Kaltenegger, L., & Sasselov, D. 2011, The Astrophysical Journal, 736, L25

Kasting, J. F., Whitmire, D. P., & Reynolds, R. T. 1993, Icarus, 101, 108

Kipping, D. M., Fossey, S. J., & Campanella, G. 2009, MNRAS, 400, 398

Kroupa, P. 2002, in Modes of Star Formation and the Origin of Field Populations. ASP Conference Series Vol. 285, ed. E. K. Grebel & W. Brandner (ASP)

Lenz, D. D., Newberg, J., Rosner, R., Richards, G. T., & Stoughton, C. 1998, ApJS, 119, 121

Moorhead, A. V., et al. 2011, The Astrophysical Journal Supplement Series, 197, 1

Muirhead, P., Hamren, K., Schlawin, E., Rojas-Ayala, B., Covey, K. R., & Lloyd, J. P. 2012, Astrophys. J., 750, L37

Pierrehumbert, R. T., Abbot, D., Voigt, A., & Koll, D. 2011, Annual Review of Earth and Planetary Science, 39, DOI:10.1146

Pinsonneault, M., An, D., Molenda-akowicz, J., Chaplan, W. J., Metcalfe, T. S., & Bruntt, H. 2012, Astrophys. J. Supp. Ser., 199, 30

Plavchan, P., Bilinski, C., & Currie, T. 2012, ArXiv e-prints

Schlegel, D., Finkbeiner, D., & Davis, M. 1998, The Astrophysical Journal, 500, 535

Selsis, F., Kasting, J. F., Levrard, B., Paillet, J., Ribas, I., & Delfosse, X. 2007, A&A, 476, 1373

Steffen, J. H., et al. 2012, The Astrophysical Journal, 756, 186

Valenti, J., & Piskunov, N. 1996, Astronomy and Astrophysics Supplement Series, 118, 595

Vanhollebeke, E., Groenewegen, M. a. T., & Girardi, L. 2009, Astron. Astrophys., 498, 95

Vickers, J. J., Grebel, E. K., & Huxor, A. P. 2012, AJ, 143, 86

von Paris, P., Grenfell, J. L., Hedelt, P., Rauer, H., Selsis, F., & Stracke, B. 2013, A&A, 549, A94

Wang, S., & Zhou, J.-L. 2011, The Astrophysical Journal, 727, 108

Williams, D. M., & Pollard, D. 2003, International Journal of Astrobiology, 2, 1

A. Derivation of a uniform probability distribution for extinction

If the probability distribution of stars with distance x along the line of sight is $f(x)$ and the density of dust is $g(x)$, then the total column density of dust along the line of sight to a particular star is

$$A = A_0 \int_0^x dx' g(x'), \tag{A1}$$

where A_0 is a constant factor. The probability of extinction to any randomly selected star falling between A and $A + dA$ is

$$p(A)dA = f(x)\frac{dx}{dA}dA. \tag{A2}$$

However, from Eqn. A1, dx/dA is simply $g(x)^{-1}$ and if $f(x)$ and $g(x)$ are identically distributed with x, then $p(A)$ is a constant, i.e. uniformly distributed over the range of allowed values.

This manuscript was prepared with the AAS LaTeX macros v5.2.

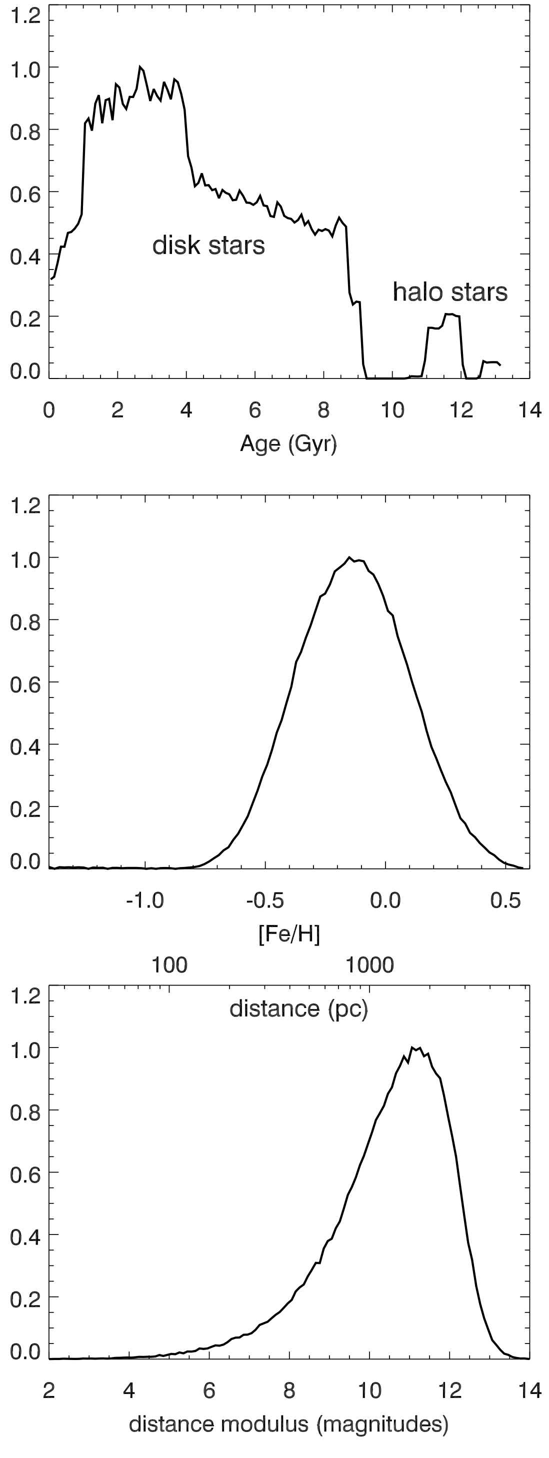

Fig. 1.— Priors of age, metallicity, and distance modulus generated from 428,792 TRILEGAL-simulated stars with $K_p < 16$ and $\log g > 4$ in the *Kepler* field. The distributions of all synthetic stars is presented here, but only the ∼10% of stars with Galactic latitudes within 0.5 deg of a *Kepler* star of interest are used to generate actual priors.

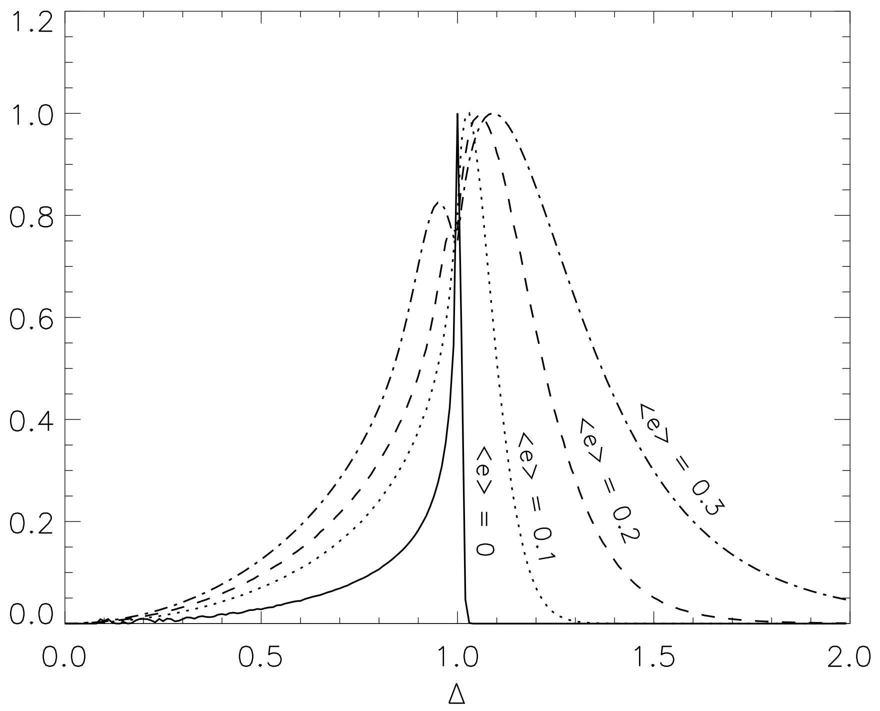

Fig. 2.— Priors on the planet transit duration as a function of the parameter $\Delta \equiv D/(\tau^{2/3} P_K^{1/3})$, where D is the transit duration, τ is the stellar free-fall time, and P_K is the Keplerian orbital period, for circular orbits (solid line) and orbits with Rayleigh-distributed eccentricities with means of 0.1, 0.2, and 0.3.

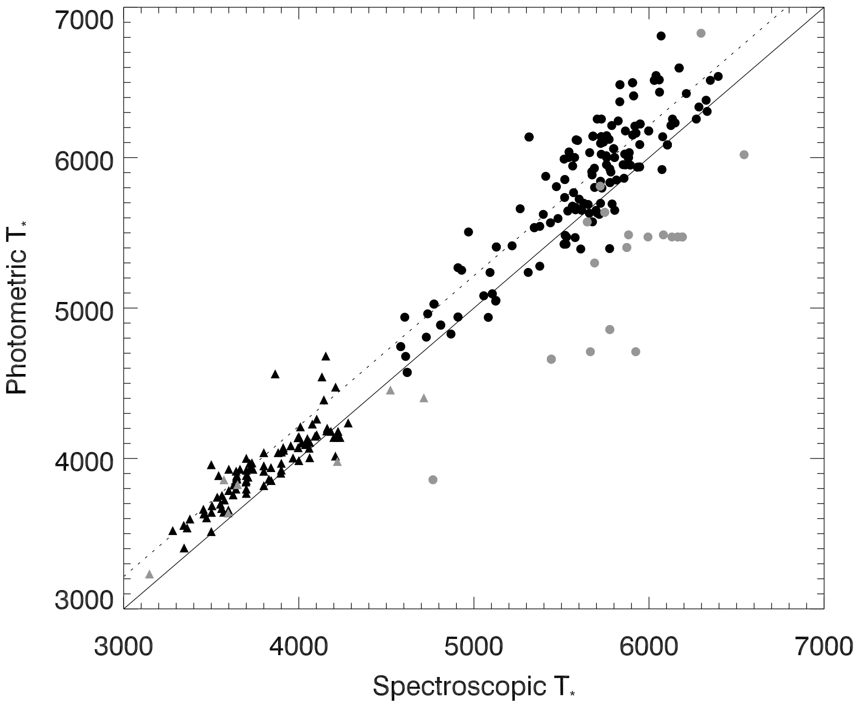

Fig. 3.— Comparison between effective temperatures based on photometry and spectroscopic values. Circles are solar-type stars from Buchhave et al. (2012) and Bruntt et al. (2012). Triangles are M dwarfs from Mann et al., in prep.. Black points are stars where all six photometric colors are available; grey points represent stars where at least one color is unavailable. The solid line is equality between the estimates and the dashed line represents the ∼215 K offset found by Pinsonneault et al. (2012).

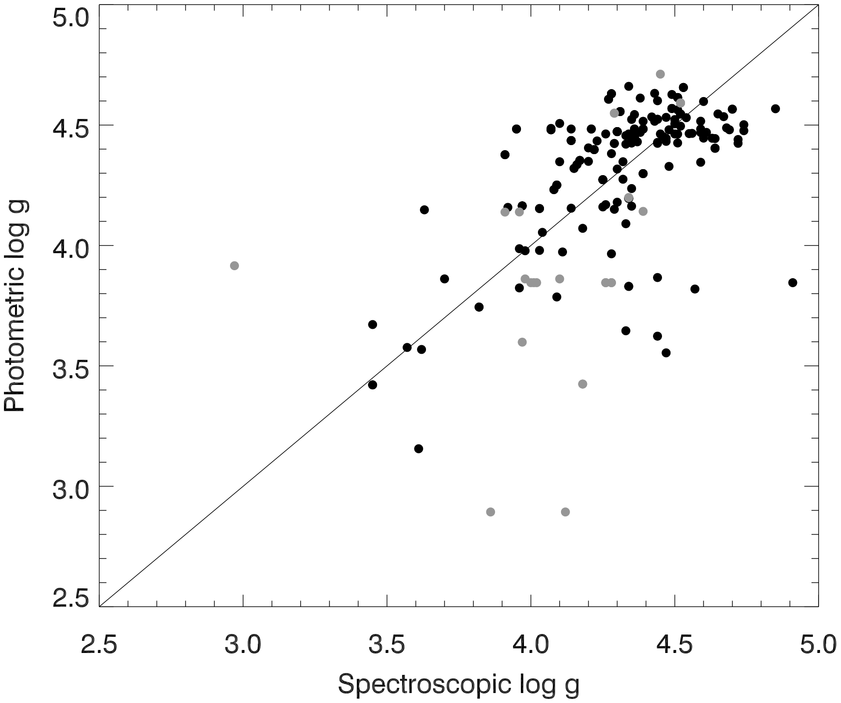

Fig. 4.— Comparison between photometric and spectroscopic estimates of surface gravities where the latter are taken from Buchhave et al. (2012) and Bruntt et al. (2012). Black points are stars where all six photometric colors are avialable; grey points represent stars where at least one color is unavailable. The solid line is equality between the two estimates.

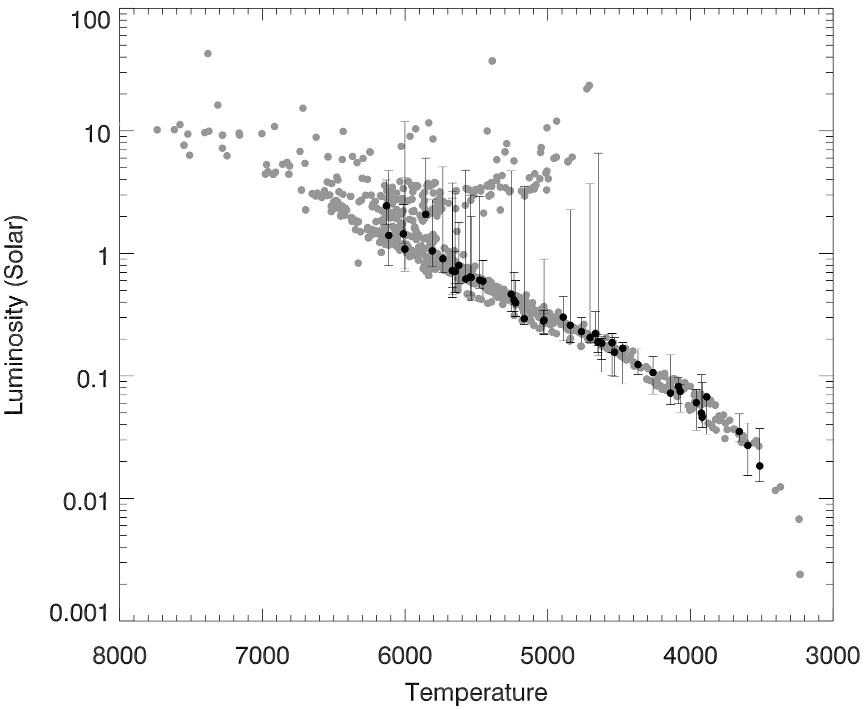

Fig. 5.— Hertzsprung-Russell diagram for host stars of 2739 candidate and confirmed *Kepler* planets. Black points are the 52 candidate HZ planets in Table 1. The error bars represent 95% confidence intervals on luminosity and are shown only for the candidate HZ planets.

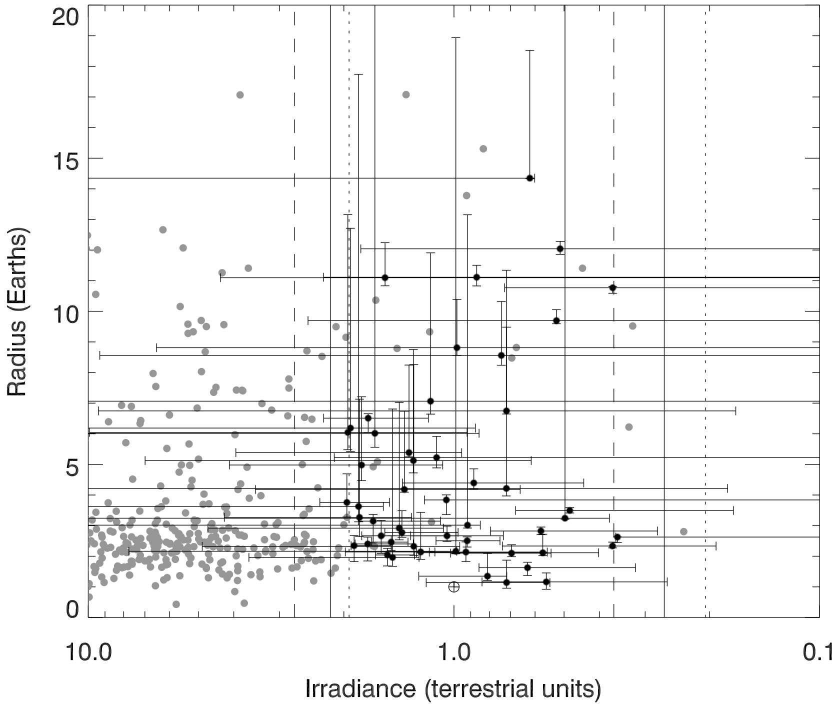

Fig. 6.— Radius and stellar irradiance of candidate and confirmed *Kepler* planets, and the Earth. Candidate planets in habitable zones are highlighted as black, all other KOIs are grey, and a the vast majority of KOIs experience higher irradiances and fall outside the left-hand boundary of the plot. The error bars correspond to 95% confidence intervals. The solid, dotted, and dashed lines are the boundaries of the HZ for a 50% cloud-covered Earth like planet around a solar-type star (5780 K), an early M dwarf (3800 K) and late A-type (7800 K) star (Selsis et al. 2007).

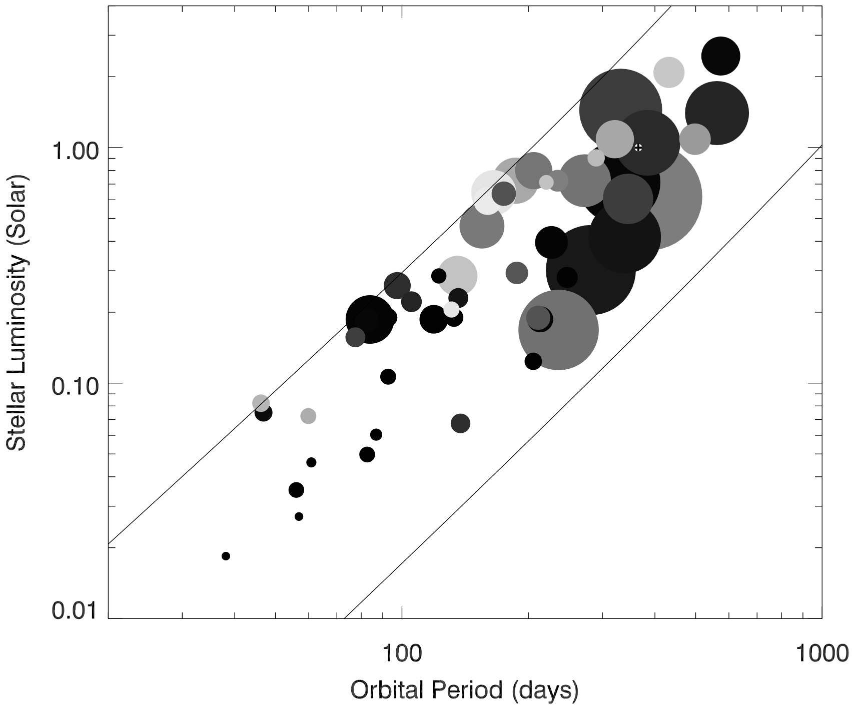

Fig. 7.— Luminosity of the host star vs. orbital period of candidate HZ planets detected by *Kepler*, plus the Earth. The points are scaled to planet radius and the the darker the point, the more likely it is in the HZ. The two lines delimit the boundaries of the HZ for Earth-like planets with 50% cloud cover (Selsis et al. 2007). To plot these boundaries with these axes, it was necessary to assume simple but standard power-law relations between the luminosities, masses, and effective temperatures of main-sequence stars.

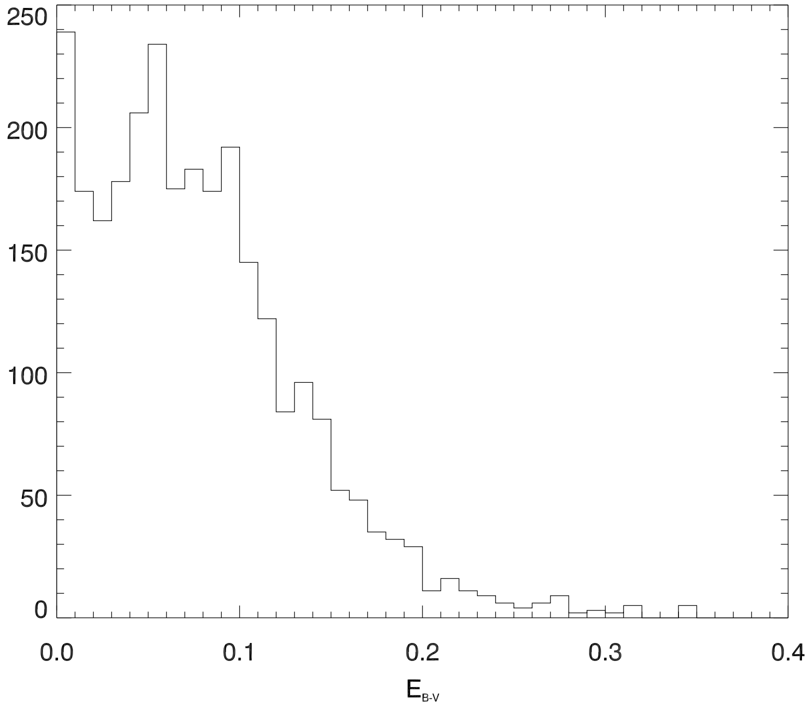

Fig. 8.— $B - V$ interstellar reddening along the line of sight to *Kepler* KOI host stars calculated using Eqn. 2 for the best-fit stellar models. The median value is 0.069.

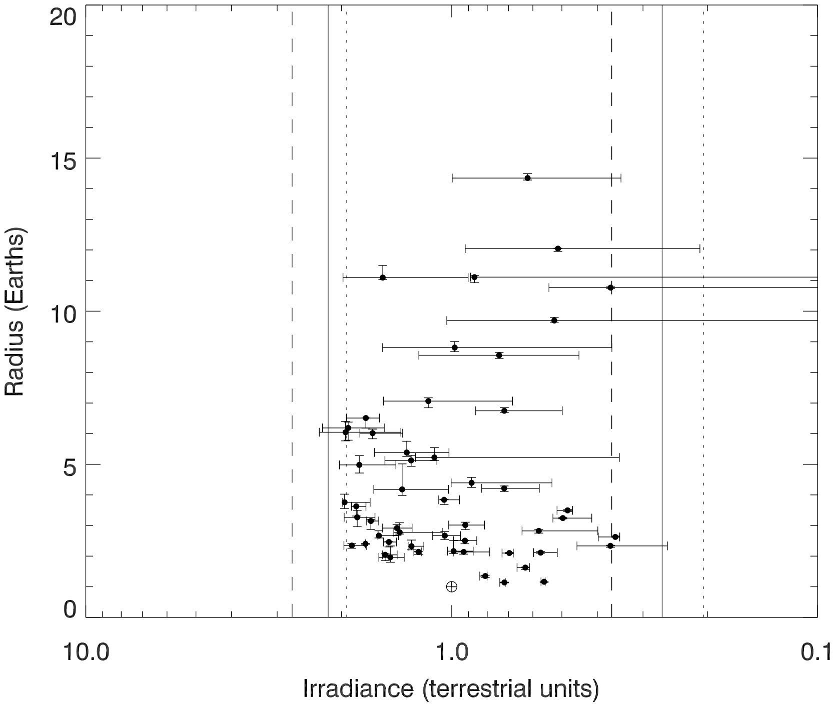

Fig. 9.— Reduction in the uncertainties in planet radius and stellar irradiation expected from inclusion of *Gaia* parallax measurements with 40 μas errors. Compare to Fig. 6.

Table 1. Candidate Planets in the Habitable Zones of *Kepler* Stars

		Planet Parameters						Stellar Parameters						
KOI	KIC	p_{HZ}	Period	Irrad.	Planet Radius ($R_\oplus$)			T_*	log g	[Fe/H]	L_*	M_*	Age	Comment[b]
			(days)	($I_\oplus$)	MP[a]	lower	upper	(K)			($L_\odot$)	($M_\odot$)	(Gyr)	
87.01	10593626	0.64	289.86	1.29	2.32	2.00	5.91	5735	4.43	-0.2	0.90	0.93	7.8	Bo11,KS11,Bu12,*Kepler*-22b
113.01	2306756	0.76	386.59	0.62	14.35	14.33	40.54	5575	4.56	-0.2	0.62	0.89	1.7	KS11,V-shaped transit
250.04	9757613	0.98	46.83	1.72	2.40	1.97	2.54	4072	4.71	-0.3	0.07	0.55	3.7	Ma13,*Kepler*-26
351.01	11442793	0.89	331.64	1.54	11.10	9.63	13.91	6012	4.34	-0.3	1.44	1.10	6.1	Bo11,KS11
371.01	5652983	0.70	498.39	0.72	4.21	3.67	19.24	6001	4.48	-0.1	1.09	1.00	1.5	
401.02	3217264	0.54	160.02	1.96	3.76	3.30	4.12	5454	4.50	-0.2	0.59	0.87	7.5	Bo11,KS11
433.02	10937029	0.99	328.24	0.87	11.11	9.58	12.52	5650	4.52	-0.2	0.71	0.92	3.7	Bo11,KS11
518.03	8017703	1.00	247.35	0.58	2.82	2.52	3.04	5030	4.63	-0.3	0.28	0.74	1.4	
622.01	12417486	0.77	155.04	1.65	6.01	5.22	23.00	5256	4.53	-0.1	0.46	0.83	7.3	Bo11,KS11
682.01	7619236	0.93	562.14	0.74	8.56	6.97	17.11	6114	4.43	-0.1	1.40	1.10	1.4	KS11,Bu12
701.03	9002278	1.00	122.39	1.52	2.04	1.80	2.16	5026	4.63	-0.3	0.29	0.72	1.2	Bo11,KS11,Bu12
812.03	4139816	0.65	46.18	1.87	2.34	1.95	2.38	4084	4.69	-0.3	0.08	0.57	4.0	Bo11,KS11,Mu12,Ma13
854.01	6435936	1.00	56.06	0.70	2.10	1.95	2.42	3658	4.79	-0.1	0.04	0.48	1.4	Bo11,KS11,Mu12,Ma13
868.01	6867155	0.78	235.97	0.37	10.77	8.16	11.13	4474	4.64	0.2	0.17	0.74	1.4	KS11,Mu12,Ma13
881.02	7373451	0.99	226.89	0.88	4.39	3.95	4.89	5225	4.57	-0.3	0.40	0.78	6.5	KS11
902.01	8018547	1.00	83.91	1.72	6.51	5.97	7.06	4623	4.63	-0.2	0.19	0.68	6.1	Bo11,KS11,Mu12
1168.01	10460629	0.61	432.13	1.37	4.18	3.47	6.30	5855	4.15	-0.1	2.09	1.35	8.5	KS11
1209.01	3534076	0.78	272.07	1.16	7.06	5.98	18.26	5668	4.50	-0.3	0.72	0.89	5.5	Ba12
1298.02	10604335	1.00	92.74	0.93	2.14	1.76	2.38	4262	4.67	-0.3	0.11	0.60	6.3	Ma13
1356.01	7363829	0.92	384.03	0.98	8.81	7.61	14.34	5809	4.41	-0.2	1.05	1.00	6.2	
1361.01	6960913	0.66	59.88	1.23	2.14	2.03	2.89	4140	4.73	-0.5	0.07	0.53	2.8	Bo11,KS11,Mu12,Ma13
1375.01	6766634	0.67	321.21	1.29	5.13	4.45	10.83	6001	4.48	-0.1	1.09	1.00	1.5	Bo11,KS11

Table 1—Continued

			Planet Parameters					Stellar Parameters						
KOI	KIC	p_{HZ}	Period (days)	Irrad. ($I_\oplus$)	Planet Radius ($R_\oplus$) MP^a	lower	upper	T_* (K)	log g	[Fe/H]	L_* ($L_\odot$)	M_* ($M_\odot$)	Age (Gyr)	Comment^b
1429.01	11030711	0.77	205.92	1.79	4.98	4.26	7.30	5623	4.45	-0.2	0.80	0.94	8.0	Bo11,KS11
1430.03	11176127	0.88	77.48	1.58	2.67	2.07	2.87	4532	4.66	-0.3	0.16	0.69	1.2	Ba12
1431.01	11075279	0.88	345.16	0.72	6.75	6.20	15.41	5477	4.50	-0.2	0.61	0.87	7.5	Ba12
1466.01	9512981	0.96	281.56	0.51	12.04	9.68	13.33	4892	4.55	0.0	0.30	0.76	11.8	Ba12
1477.01	7811397	0.97	339.08	0.52	9.70	8.47	11.68	5236	4.56	-0.2	0.42	0.82	6.0	KS11
1574.02	10028792	0.99	573.96	1.12	5.22	3.99	6.23	6131	4.19	-0.2	2.45	1.32	6.0	
1582.01	4918309	0.67	186.40	1.92	6.19	5.14	14.62	5668	4.50	-0.3	0.72	0.89	5.5	Bo11,KS11
1596.02	10027323	0.93	105.35	1.39	2.78	2.36	2.94	4666	4.62	0.2	0.22	0.77	1.8	Bo11,KS11,Mu12
1686.01	6149553	1.00	56.87	0.56	1.16	0.86	1.44	3598	4.84	-0.2	0.03	0.44	1.8	Ba12,Ma13
1739.01	7199906	0.62	220.66	1.47	1.96	1.74	4.13	5650	4.52	-0.2	0.71	0.92	3.7	Ba12
1871.01	9758089	1.00	92.72	1.48	2.46	2.31	2.65	4649	4.64	-0.2	0.19	0.71	1.4	Ba12
1876.01	11622600	0.99	82.53	1.66	3.15	2.57	3.31	4622	4.64	-0.2	0.18	0.72	2.1	Ba12
1902.01	5809954	0.91	137.87	0.36	2.63	1.93	2.63	3886	4.71	0.2	0.07	0.58	1.0	Ba12,Ma13
2102.01	7008211	0.83	187.75	0.92	3.01	2.94	12.37	5165	4.62	-0.5	0.29	0.68	7.7	Ba12
2418.01	10027247	1.00	86.83	0.63	1.62	1.31	1.85	3959	4.74	-0.4	0.06	0.53	1.2	Ba12,Ma13
2469.01	6149910	0.55	131.19	0.99	2.16	2.17	8.92	4704	4.64	-0.2	0.21	0.73	1.6	Ba12
2626.01	11768142	1.00	38.10	0.72	1.14	0.97	1.61	3514	4.90	-0.3	0.02	0.38	1.5	Ba12,Ma13
2681.01	6878240	0.62	135.49	1.33	5.38	5.01	8.00	5026	4.63	-0.3	0.29	0.72	1.2	
2686.01	7826659	0.84	211.04	0.50	3.24	3.12	21.08	4647	4.64	-0.2	0.19	0.70	1.5	
2689.01	10265602	0.56	165.35	1.95	6.04	5.01	14.01	5544	4.53	-0.1	0.64	0.92	3.5	
2691.01	4552729	0.91	97.46	1.82	3.63	3.36	12.11	4842	4.62	-0.2	0.26	0.75	1.6	
2703.01	5871985	0.99	213.26	0.48	3.49	3.18	3.69	4549	4.63	0.2	0.19	0.71	1.1	

Table 1—Continued

			Planet Parameters					Stellar Parameters						
KOI	KIC	p_{HZ}	Period (days)	Irrad. ($I_\oplus$)	Planet Radius (R$_\oplus$) MP[a]	lower	upper	T_* (K)	log g	[Fe/H]	L_* ($L_\odot$)	M_* ($M_\odot$)	Age (Gyr)	Comment[b]
2757.01	6432345	0.75	234.63	1.41	2.92	2.57	6.21	5668	4.50	-0.3	0.72	0.89	5.5	
2762.01	8210018	1.00	132.99	0.92	2.50	2.33	2.70	4647	4.64	-0.2	0.19	0.71	1.6	
2770.01	10917043	1.00	205.38	0.37	2.33	2.16	2.70	4368	4.68	-0.3	0.12	0.62	1.2	Ba12
2834.01	5609593	0.96	136.21	1.04	2.67	2.35	2.94	4764	4.63	-0.1	0.23	0.74	1.5	
2933.01	12416987	1.00	119.08	1.05	3.84	2.72	3.99	4549	4.63	0.2	0.19	0.71	1.1	
2992.01	8509442	1.00	82.66	0.57	2.11	1.94	2.81	3923	4.77	-0.4	0.05	0.50	2.0	
3010.01	3642335	1.00	60.87	0.81	1.35	1.26	1.79	3918	4.79	-0.5	0.05	0.49	2.0	
3086.01	10749059	0.84	174.74	1.81	3.27	2.76	5.70	5537	4.53	-0.1	0.64	0.91	3.3	
Other Planets with $R_p < 2\mathrm{R}_\oplus$ and $p_{HZ} > 0.1$														
775.03	11754553	0.13	36.45	2.50	1.93	1.73	2.16	4132	4.71	-0.4	0.08	0.56	3.6	Bu12,
1422.02	11497958	0.39	19.85	2.39	1.85	1.34	2.01	3638	4.83	-0.3	0.03	0.45	1.4	
2124.01	11462341	0.36	42.34	2.42	1.19	1.05	1.41	4229	4.70	-0.4	0.10	0.59	1.5	Ba12,Ma13
2650.01	8890150	0.48	34.99	2.77	1.61	1.12	1.63	4039	4.67	0.1	0.09	0.61	5.5	Ba12
2931.01	8611257	0.20	99.25	2.31	1.89	1.68	7.60	5126	4.61	-0.2	0.35	0.79	1.5	
3034.01	2973386	0.46	31.02	2.11	1.61	1.40	2.01	3923	4.77	-0.4	0.05	0.50	2.0	

[a] MP = most probable radius

[b] Reported as HZ candidate in: B11 = Borucki et al. (2011), KS12 = Kaltenegger & Sasselov (2011), Ba12 = Batalha et al. (2012); Spectroscopy reported in Bu12 = Buchhave et al. (2012), Mu12 = Muirhead et al. (2012), Ma13 = Mann et al., in prep.